Accepted Manuscript

Seismogenesis and earthquake triggering during the 2010–2011 Rigan (Iran) earthquake sequence

Hiwa Mohammadi, Thomas J. Bayliss, Esmaeil Nekouei Ghachkanlu

PII: S1464-343X(16)30378-8

DOI: 10.1016/j.jafrearsci.2016.11.019

Reference: AES 2732

To appear in: *Journal of African Earth Sciences*

Received Date: 10 March 2016

Revised Date: 7 November 2016

Accepted Date: 18 November 2016

Please cite this article as: Mohammadi, H., Bayliss, T.J., Nekouei Ghachkanlu, E., Seismogenesis and earthquake triggering during the 2010–2011 Rigan (Iran) earthquake sequence, *Journal of African Earth Sciences* (2016), doi: 10.1016/j.jafrearsci.2016.11.019.

Seismogenesis and earthquake triggering during the 2010–2011 Rigan (Iran) earthquake sequence

Corresponding Author: **Hiwa Mohammadi**

Order of Authors: Hiwa Mohammadi [1], Thomas J. Bayliss [2], Esmaeil Nekouei Ghachkanlu[1]

1. **Department of Earth Sciences, College of Sciences, Shiraz University, Shiraz, Iran**

   E-mail: Hiwa.2006.waran@gmail.com

2. **Seismic Risk Group, School of Environmental Sciences, University of East Anglia, Norwich, Norfolk NR4 7TJ, United Kingdom.**

Abstract

This study assesses the aftershock activity of two earthquakes that occurred on December 20, 2010 with magnitude of M_N 6.5 (Global CMT M_w 6.5) and January 27, 2011 with magnitude of M_N 6.0 (Global CMT M_w 6.2) in the Rigan region of southeastern Iran. This study has been done by assessing the statistical properties of the aftershock sequences associated with each of these earthquakes, namely *b*-value of Gutenberg–Richter relation, partitioning of radiated seismic energy, *p*-value of modified Omori law and the D_C-value associated with the fractal dimension. The *b*-values of *b*=0.89±0.08 and *b*=0.88±0.08 were calculated for first main shock and second main shock sequence respectively. This suggests that this region is characterized by large differential stress; the genesis of large aftershock activity in a short time interval gives power this. Further, 2.2% of the whole energy is related with the aftershocks activity for first main shock sequence while 97.8% is associated with main shock; for second sequence , 20% of the total energy is associated with the aftershocks activity while 80% is associated with main shock. The *p*-values of 1.1±0.12 and 1.1±0.1 were calculated for first and second main shocks sequence respectively, which imply fast decay rate of aftershocks and high surface heat flux. A value of the spatial fractal dimension (D_c) equal to 2.34 ± 0.03 and 2.54 ± 0.02 for first and second main shocks sequence respectively, which reveals random spatial distribution and source in a two-dimensional plane that is being filled-up by fractures. Moreover, we then use the models to calculate the Coulomb stress change to appraise coming seismic hazard by inspecting the static Coulomb stress field due to these two main shocks for the recognition of the conceivable regions of aftershocks activity. The first main shock increased stress by more than 0.866 bars at the hypocenter of the second main shock, thus promoting the failure. In addition, the cumulative

coseismic Coulomb stress changes due to the reveals that most of the aftershocks happened in the region of increased Coulomb stress.

Keywords: Rigan, Statistical properties of aftershocks, b-value, partitioning of radiated seismic energy, Omori law, spatial fractal dimension (D_c), Coulomb failure stress.

1. Introduction

On December 20, 2010 at 22:12 local time, a moderately-sized earthquake of M_N 6.5 (Global CMT M_w 6.5) took place near Rigan in southeastern Iran. Thirty-eight days later, another moderately-sized earthquake M_N 6.0 (Global CMT M_w 6.2) occurred nearby on January 27, 2011 at 12:09 local time on January 27 2011. The Rigan area is located in southeastern Iran, at the southern segment of the Lut block and the northern border of the Jazmourian depression (Fig. 1). The first main shock resulted in four deaths, all in the low settlement of Chah Qanbar; no casualties were narrated from the 2011 event (Walker et al. 2013). The historical seismicity (Fig. 1) of this area is limited to the earthquakes reported after 1800 A.D. (Ambraseys and Melville, 1982; Berberian, 1995). Berberian (1995) suggests evidence may be present for historical earthquakes around Koohbanan, Zarand, Kerman, Bam and Mahan caused by active faults near them. Important historical earthquakes are the Nosrat-Abad (1838), Hoorjand (November, 1854), Chatrood (January, 17, 1864), Chatrood (August, 4, 1871) and Sirch (1877). The M_S = 7.0 Nosrat-Abad earthquake was a shock followed by two years of aftershocks. The M_S= 5.8 (MMI = VII+) Hoorjand earthquake destroyed some villages located northeast of Kerman. More recently Iranian seismic activity has been documented on in-situ recording equipment, notably during the 2003 Bam (M_w=6.6) and 1998 (M_S=5.3) earthquakes with known mechanisms and the 1923 (M_S=5.6) with unknown focal mechanism which related to the Kahourak fault.

The Lut block is placed in southeastern Iran and expands approximately 200 km east to west and almost 900 km north to south, and is commonly regarded as a non-deforming tectonic structure. It is bordered to the south by the Jazmourian depression, to the north by the Doruneh fault, to the west by the Nayband fault and the Gowk fault system and the Nehbandan fault system in the east (Hessami and Jamali, 2006). The Gowk, Sabzevaran, Bam, Jiroft and the Nehbandan (including Kahurak F., southwest termination) fault zones are the seismically active fault systems close to the epicentral area considered in this study. Rezapour and Mohsenpur (2013) state that December 20, 2010 Rigan earthquake started by enactment of a dextral fault in the upper crust. They also state that the geometries of the conceivable activated fault planes match the Kahurak and Bam faults in the area, while a clear alignment of the epicentral distribution of the aftershocks recorded by the temporary seismic network are consistent with the Kahurak fault trend. However, Ashtari-Jafari (2011) determined that the first main shock happened on a hidden earthquake fault, running approximately parallel to the Bam earthquake fault, and he recommended the name 'Rigan earthquake fault' for this new fault. These events provide opportunity to further understand the distribution of active faults in the region and the seismic hazard local populations may be subject to. The earthquakes additionally offer a new perception into the active tectonics of this region as well as 2003 Bam earthquake (M_w =6.6).

Many estimates of the locations of each main shock have been made. The Institute of Geophysics at University of Tehran (IGUT) estimated the locations using their permanent seismic stations-at 28.44^{o}N and 59.15^{o}E for the first main shock, and second main shock at 28.294^{o}N and 58.95^{o}E. The focal mechanism solutions from different seismological agencies were published after the both main shocks occurred. Walker et al. (2013) used interferometry and teleseismic body waveform and surface displacements from Synthetic Aperture Radar (SAR) interferometry to suggest the 2010 main shock induced with a right-lateral strike-slip motion on a formerly near-vertical fault with a strike of ~210°N;, and that the 2011 main shock induced with a left-lateral strike-slip motion on another near-vertical fault with strike of ~310°N. While they successfully identified a series of tiny cracks and en-echelon fissures that appeared after these earthquakes, neither event created a good visible surface trace in the region. However, U.S. Geological Survey's (USGS) solution was to suggest a right lateral strike-slip including a reverse component; the Global Centroid Moment Tensor (Global CMT) solution for the first main shock provided by the Harvard group is in agreement with a pure dextral strike-slip motion. Based on USGS and Global CMT outcomes, northeast–southwest and trends northwest–southeast were proposed for nodal planes.

Earthquakes are typically followed by increased seismic activity, identified as 'aftershocks', which last for several days to several years. They are also subject to complicated triggering mechanisms which move in a highly heterogeneous system of non-linearly cooperation faults incorporated in a visco-elastic medium (Ben-zion, 2008); relaxation of these stresses motivates aftershocks (Rybicki, 1973; Mendoza and Hartzell, 1988; King et al., 1994; Hardebeck et al., 1998). This analysis evaluates aftershock activity using a range of statistical properties of aftershock sequences (*b*-value of Gutenberg–Richter relation, partitioning of radiated seismic energy, *p*-value of modified Omori law, and D_C- value of fractal dimension) in order to shed light on the seismotectonic properties of the study area. In addition, an attempt has been made to assess future seismic hazard by examining the static Coulomb stress field due to coseismic slip of both main shocks for the identification of the possible regions of aftershocks activity.

2. Tectonic Setting

The Alpine–Himalayan belt in Iran is represented by a wide band of diffused seismicity and includes a few mobile belts encompassing little and fairly steady blocks. Berberian (1976) separated Iran into four major seismotectonics zones, one of which is the major component of the Central Iranian Block, which includes of the Lut , Poshte Badam, Yazd and Tabas blocks. The boundaries among these blocks are strike slip faults, the blocks have been liable to extensive counter-clockwise rotation. Also, the fault systems in this region are varied from those in other parts of Iran because of the orientation and geometric specification of the faults; for example, they are linear, long, and narrow (Hessami and Jamali, 2006). The latest dynamic deformation in the east central Iran is overwhelmed by major N–S or NNW–SSE right-lateral strike slip faulting with some NW–SE reverse faults and some E–W left-lateral strike–slip faults. The northward movement of central Iran in respect to western Afghanistan results in local scale right-lateral shear across the eastern border of Iran, which is located south of latitude 34◦N on N–S right-lateral faults that surround the Dasht-e-Lut (Walker and Jackson, 2004; Meyer and Le Dortz, 2007). The Central Iran is not considered a linear seismic zone. It is portrayed by scattered seismic movement with large-Earthquakes generated in central Iran are typically shallow focus (less than 25 km) and are normally associated with surface faulting (Berberian, 1976). The 2010 and 2011 Rigan earthquakes occurred in the low-lying and sparsely inhabited Narmashir desert district region south of the Dasht-e-Lut desert. This region is flanked toward the south by the

Shahsavaran mountains mountain chain. The epicentral region of these events was situated between the southern Lut Block and the Makran–Jazmourian Depression. Various large earthquakes happened on the right-lateral strike–slip fault systems along the western edge of Dasht-e-Lut. Walker (2006) proposed that Late-Quaternary thrust faulting and strike-slip faulting occurred inside of the area, that regional faults are imperative to allow exchange of tectonic strain by appropriating a part of the right-lateral shear among the Makran-Zagros districts along the right lateral fault systems toward the central parts of Iran.

3. Rigan main shocks and their aftershock sequence

The earthquake catalogue used in the current study is taken from the Iranian Seismological Center of the Institute of Geophysics at University of Tehran (IGUT; http://irsc.ut.ac.ir/bulletin.php/). An earthquake data set used in seismicity or seismic hazard studies surely should be homogenous. In other words, it is indispensable to apply the equal magnitude scale in seismic analyzes. The IGUT reported earthquakes on the corrected Nuttli (1973) magnitude (M_N) scale. However, the study area is located in the SE of Iran between longitudes of 57.00-59.00°E and latitudes of 28.00-29.00°N on which the events occurred. Figure 2 shows the epicenter locations of the main shocks and their aftershocks. This sequence consists of 256 earthquakes of $2.6 \leq M_N \leq 6.5$ recorded by IGUT during the period December 20, 2010 to April 6, 2011. Figure 3a displays the cumulative number of earthquakes with $M_N \geq 2.6$ in the catalog. The seismicity rate has a sharp change after the first main shock (red star in Fig. 2) which occurred on December 20, 2010 with M_N=6.5 and at the second main shock which occurred on January 27, 2011 with magnitude M_N= 6.0 (Yellow Star in Fig.2) due to the Rigan aftershock sequence. Figure 3b illustrates magnitude of events versus time. We can see that there are two main clusters in this sequence, each occurring in the days following each of the main shocks considered in this work. Thus, here we defined two sequences, first sequence has been considered after occurrence December 20, 2010 till before occurrence second main shock and second sequence has been considered after occurrence second main shock from January 27, 2011 till 6 April 2011. Most of the aftershocks from first main shock are clustered in the NE to SW direction (Fig. 3c) coinciding with the strike of one of the nodal plane (np1 strike = 36, dip = 87, rake = 180) of the first main shock's fault plane solution reported in the Global CMT catalogue. IGUT reported 15 aftershocks of magnitude $M_N \geq$ 4.0 within first sequence which mainly declusterd NE to SW (Fig. 3c). The occurrence of such larger magnitude aftershocks in any aftershock sequence suggests that large asperities exist in the rupture zone of main shock from where seismic energy is released in the form of moderate size aftershocks. Also, aftershocks associated with the second main shock are mainly declustered in the NW to SE direction (Fig. 3d) coinciding with the strike of one of the nodal plane (np1 strike = 129, dip = 77, rake = −5) of the second main shock's fault plane solution reported in the Global CMT catalogue. IGUT reported 17 aftershocks of magnitude $M_N \geq$4.0 within this sequence and mainly declusterd NW to SE. Also, Walker et al. (2013) state that the causative fault of the December 20, 2010 has NE to SW direction and January 27, 2011 Rigan earthquakes has NW to SE direction.

4. Statistical properties of the aftershock sequence

4.1. Frequency–magnitude scaling relationship

The quantity *N* of earthquakes with magnitudes larger than or identical to *M* is approximated by using the relation (Gutenberg and Richter, 1944):

$$log_{10}N_m = a_m - bM \qquad (1)$$

where N_m is the cumulative number of earthquakes with magnitudes equal to or large than *M*, *b* depicts the slope of the size distribution of events, and *a* is corresponding to the seismicity rate. Appraisals of *b*-value intimate a fractal relation among frequency of occurrence and the radiated energy, seismic moment or fault length, and this is one of the most extensively used statistical parameters to explain the scale scaling properties of seismicity. The *b*-value for the most part fluctuates from 0.5 to 1.5 contingent upon the tectonic setting, tectonic stress and the magnitude ranges, but regularly approaches to 1 for seismically active regions. The variety of *b*-value can be identified with the stress distribution after the main shock, as well as the history of previous ruptures. Spatial and temporal varieties in *b*-values are distinguished to reflect the stress field, for the *b*-value is conversely reliant on differential stress (Scholz 1968; Ogata et al., 1991; Urbancic et al., 1992; Ogata and Katsura, 1993; Narteau et al., 2009). Schrolemmer et al. (2005) state that the *b*-value is additionally subject to styles of faulting, as the *b*-values of thrust faults are the lowest among the three types of faulting mechanisms, which can be considered as confirmation of the relationship between *b*-value and stress. Areas with lower *b*–value are likely to be areas under higher applied shear stress after the main shock, while the areas with higher *b*–value are areas that encounter slip. Estimation of reliable *b*-values is reliant on a clearly defined time interval of catalogued seismicity.

There are many techniques to estimation *b*-value; yet the most powerful and generally acknowledged technique for estimation of *b*-value is the Maximum Likelihood Method (MLM). The *b*-value of a region can be assessed from the aftershock sequence data utilizing the hypothetical thought given as Utsu (1965):

$$b = \frac{Log_{10}e}{M_{mean} - M_c} \qquad (2)$$

As shown in Fig. 4, the cut-off magnitude (M_c) for the both sequences was calculated to be equal to 3.2 with 90% goodness of fit level (Fig. 4); the frequency-magnitude statistics of theses aftershocks sequence were modeled using the GR scaling relation. For the first aftershock sequence, from December 20, 2010 to January 27, 2011, *b*=0.89 $\pm$ 0.08 and *a*=4.77 (Fig. 4a) were calculated; similarly, *b*=0.88 $\pm$ 0.08 and *a*=4.86 (Fig. 4b) were calculated for the second main shock sequence. The *b*-value in both sequences are lower than the global mean value of 1.0, suggesting that the two sequences are subject to larger magnitude aftershocks and high differential crustal stress in the regime.

4.2. Energy partitioning

Utsu (2002) claims that the level of aftershocks is chiefly related with the size of main shock in a seismic sequence. The stress situation and heterogeneity of rock mass influences the change in size (Δm) between magnitude of main shock (M_{ms}) and its biggest aftershock. In its unique structure, Båth's law expresses that the difference Δm between a given main shock with magnitude M_{ms} and its biggest aftershock magnitude is constant, independent of the main shock magnitude (Båth, 1965). However, in spite of extensive research about the statistical variability of Δm (Vere-Jones, 1969; Kisslinger and Jones, 1991; Console et al., 2003), the validity of the law remains an open issue (Vere-Jones, 1969; Vere-Jones et al., 2005). This study aims to derive the biggest aftershock magnitude from the Gutenberg-Richter law and fit it into the standard view of Bath's law following Shcherbakov and Turcotte (2004).

The magnitude of the biggest aftershock consistent with Gutenberg-Richter relationship for aftershocks is obtained by assuming $N\ (\geq m) = 1$ which yields $a = bm^*$. If Båth's law is applicable to the inferred magnitude m^* the Gutenberg–Richter relationship takes the following form:

$$log_{10}N(\geq M) = b(M_{ms} - \Delta m^* - M) \qquad (3)$$

where $\Delta m = M_{ms} - M^*$. The energy E radiated throughout an earthquake is associated empirically to its moment magnitude M by (Utsu, 2002)

$$log_{10}E(M) = \frac{3}{2}M + log_{10}E_0 \qquad (4)$$

With, E_0 = 6.3 × 104 Joules.

This relation is applied directly to describe the link among the energy radiated by the main shock E_{ms} and the moment magnitude of the main shock M_{ms},

$$E_{ms} = E_0 . 10^{\frac{3}{2}m_{ms}}$$

Shcherbakov and Turcotte (2004) state that the proportion of the whole radiated energy by the aftershocks E_{as} to the whole energy radiated by the main shock E_{ms} is given by

$$\frac{E_{as}}{E_{ms}} = \frac{b}{\frac{3}{2}-b} 10^{-\frac{3}{2}\Delta m} \qquad (5)$$

Assuming that all earthquakes have the same seismic efficiency, the share of the radiated energy to the whole is saved as elastic energy is also the proportion of the drop within the stored elastic power due to the aftershocks to the drop in the stored elastic energy because of the main shock. Shcherbakov in et al. (2005) determined the fraction of entire energy associated with aftershocks can be written as

$$\frac{E_{as}}{E_{ms}+E_{as}} = \frac{\frac{b}{\frac{3}{2}-b} 10^{-\frac{3}{2}\Delta m}}{1+\frac{b}{\frac{3}{2}-b} 10^{-\frac{3}{2}\Delta m}} \qquad (6)$$

Therefore, by considering a = 4.77 and b = 0.89 for first sequence and a = 4.86 and b = 0.88 for second sequence which computed from G–R relationship, the modified magnitude for the largest aftershock (M^*) as 5.3 and 5.5 for the first and second sequences respectively. Moreover, magnitude difference (Δm^*) as 1.2 and 0.5 for first and second sequences respectively. We found that 2.2% of the whole energy is related with the for first sequence's aftershock activity while 97.8% is associated directly with main shock. In comparison, 20% of the total energy is associated with the aftershock activity from the second sequence while 80% is associated with main shock.

4.3. Temporal decay of aftershock events

Aftershock activity will decay over time in a quasi-hyperbolic manner. This decay is typically described by using a relation known as the changed Omori law (Utsu et al., 1995; Ben-Zion, 2008) expressed inside the equation:

$$n(t) = k(t + c)^{-p} \qquad (7)$$

where n(t) is the occurrence rate of aftershocks (number of shocks/day), t-days after the main shock; k, c and p are positive constants. To determine those parameters, it is common to make use of the cumulative range of aftershocks (Utsu, 2002) inside the form:

$$N(t) = \frac{k[c^{1-p} - (t+c)^{1-p}]}{p-1} \qquad for\ p \neq 1 \qquad (8)$$

where *N(t)* is the cumulative number of aftershocks t-days after the main shock. However, the most important is generally considered to be p, with p = 1 in the original version of the Omori law. According to Olssen (1999) and Utsu et al. (1995), p changes between 0.5 and 1.8, and this parameter varies from sequence to sequence based to tectonic situation in the examined area. In this manner, more consideration is paid in the estimation p utilizing the maximum likelihood as suggested by Nyffengger and Frolich (1998, 2000). k is controlled by aggregating the number of events in the sequence. c which usually approximates to zero, is a dubious parameter (Utsu et al., 1995) and is dependent on the rate of activity in the beginning part of the sequence. Clearly, if c = 0, *n(t)* in Eq. (7) diverges at t = 0. According to Yamakawa (1968), higher values for c (c ≥ 0.01 days) imply more complex capabilities of the rupture process of the main shock. Whilst p is sort of unbiased of the threshold magnitude, M_c, c often suggests tight dependence on M_c (Utsu, 2002). This is probably because of missing data shortly after the main shock when considerable small aftershocks are not seen on reported records. The reason for fluctuating values of p in the crust is inadequately known. Moreover, the aftershock decay is thought to mirror the strain readjustment following the strain changes because of the main shock (Ben-Zion, 2008). Stress readjustment can be considered to mirror the complicated relaxation processes (Stein and

Wysession, 2002), and structural heterogeneity within the source volume (Kisslinger and Jones, 1991; Utsu et al., 1995) associated to the tectonic structure of the region.

The maximum likelihood method was applied to estimate the value of *p* of Eq. (7) for the aftershock sequence of the Rigan sequence shown in Fig. 5. The *p*-values of 1.1 ± 0.12 (Fig. 5a) and 1.1 ± 0.1 (Fig. 5b) were calculated for the first and second sequence respectively. The *p*-values are higher value compared to the usual values of the order of 1.0 (Fig. 5). Bowman (1997) determined that the temporal decay of aftershock activity indicates the strain scattering with time in the aftershock region for intraplate earthquakes in Australia. Kisslinger and Jones (1991) related high *p*-values to high estimations of heat flow for California and proposed that higher temperature created abbreviated stress slackening times for the fault zone.

4.4. Spatial fractal dimension

Seismicity is a classical instance of a complicated phenomenon that may be quantified the usage of fractal theory (Turcotte, 1997). Specifically, epicenter distributions and fault networks have fractal properties (Goltz, 1998). The fractal dimension (D) qualities are evaluated utilizing the connection dimension. The correlation dimension as characterized by Grassberger and Procaccia (1983) measures the spacing of the set of points, which in this example are the earthquake epicenters and is given as:

$$D_c = \lim_{r \to 0}[logC(r)/logr] \quad (9)$$

where C(r) is the correlation function. The correlation function measures the clustering or spacing of a set of factors, here the earthquake epicenters, and is given via the relation:

$$C(r) = \frac{2}{N(N-1)} N(R < r) \qquad (10)$$

where N(R/r) is the number of pairs (Xi, Xj) with a smaller distance than r. Should the epicenter dispersion have a fractal structure, the subsequent relation is acquired

$$C(r) \sim r^D \qquad (11)$$

where D is a fractal dimension, more strictly, the correlation dimension (Grassberger and Procacci, 1983). The usage of this relation the fractal dimension of spatial distribution of the earthquakes is evaluated. By plotting C(r) towards r on a double logarithmic coordinate, the fractal size D is detrermined by the graph's slope. The distance r between two events, ($\Theta 1$, $\phi 1$) and ($\Theta 2$, $\phi 2$), is calculated by using a spherical triangle as given by Hirata (1989):

$$r = cos^{-1}\,[cos\Theta 1 cos\Theta 2 + sin\Theta 1 sin\Theta 2 cos(\phi 1 - \phi 2) \qquad (12)$$

The slope is obtained by fitting a least-square line in the scaling region.

The spatial fractal dimension for the Rigan sequence is calculated from the double-logarithmic plot of the correlation integral and distance between hypocenters (Fig. 6), and found to be equal to 2.34 ± 0.03 (Fig. 6a) and 2.54 ± 0.02 (Fig. 6b) for the first and second sequence respectively. The D_c-value is larger than 2.0 in both sequences, indicating that the events are randomly distributed into the fault zone crustal volume, whereas much of this volume seems free from hypocenters.

5. Static Coulomb-stress changes

In recent years, various studies have investigated the Coulomb stress change to clarify the earthquake interactions worldwide (Stein et al., 1994; Harris, 1998; Nalbant et al., 1998; Shen et al., 2003; Papadimitriou and Sykes, 2001; Papadimitriou et al., 2004, 2007; Liu et al., 2007; Chen et al., 2008; Gkarlaouni et al., 2008; Han et al., 2008; Karakostas et al., 2013), the aftershock distribution (Stein and Lisowski, 1983; King et al., 1994; Deng and Sykes, 1997; He et al., 2013; Chan and Wu, 2014), and the stress change on target faults (Sarkar and Chander, 2003; Parsons et al., 2008; Toda et al., 2008; Wan et al., 2010; He et al., 2011; Li et al., 2013; Qian and Han, 2013). The interaction between large earthquakes may be considered a source of earthquake triggering, and the aftershock distribution may be defined by the Coulomb failure criterion. Aftershocks are plentiful in which the Coulomb failure pressure increases and sparse where the Coulomb failure pressure decreases. Furthermore, the Coulomb failure stress changes have established quite efficient at figuring out the locations of large earthquakes in the surroundings. However, Coulomb failure stress change (ΔCFF) may be clearly expressed as (Freed, 2005; Harris, 1998; King and Cocco, 2000; King et al., 1994; Stein et al., 1994; Toda et al., 1998):

$$\Delta CFF = \Delta\tau + \mu'(\Delta\sigma + \Delta P) \qquad (13)$$

where $\Delta\tau$ is the shear stress change along the slip direction on the assumed fault plane, μ is the coefficient of friction, $\Delta\sigma$ is the normal stress change, and ΔP is the change in pore fluid pressure. Stress changes were computed on receiver planes due to rectangular dislocations in a uniform, elastic half-space with a Poisson's ratio of 0.25 and shear modulus of 3.3×10^4 MPa. However, for a strike-slip fault, μ is commonly considered to be low (e.g., 0.4), whereas for a continental thrust μ is generally higher (up to 0.8) (King et al., 1994). Lower obvious coefficient of friction ought to arise if the fault has encountered more cumulative slip (Parsons et al., 1999). However, μ = 0.4 was used in these stress calculations based on the coseismic elastic dislocation modelling of the earthquakes (Okada, 1992) by assuming earthquake ruptures as rectangular dislocation surfaces in an elastic half-space having Young's modulus of 8×10^5 bar and Poisson's ratio of 0.25. Coulomb 3.3 software was used to calculate Coulomb failure stress changes (Lin and Stein, 2004; Toda et al., 2005).

To understand whether the first main shock changed the proximity to failure on the second main shock fault, the change in the Coulomb stress associated with the first main shock may encourage or discourage the main shock fault was examined. The first main shock of magnitude M_N 6.5 occurred NE of the second main shock epicenter with magnitude M_N 6.0. The NE–SW trending plane is considered as the fault plane of first main shock. The stress changes caused by the first main shock are shown in Fig. 7. The Coulomb stress change due to the first main shock fault (rp1 strike = 36°, dip = 87°, rake = 180°) was calculated on the second main shock receiver fault (rp1strike = 129°, dip = 77°, rake = −5°). At first glance, in Fig. 7, the stress-increased or bright zone can accelerate the seismicity while the stress-shadow zone can decelerate. It is observed that the second main shock epicenter of magnitude M_N 6.0 took place in the lobe of increased (positive) Coulomb stress which shows that second main shock was promoted to failure due the transfer of positive Coulomb stress by coseismic slip of first main shock and thus triggered by first main shock. The calculated Coulomb stress changes due to first main shock, in a cross-section along line AB passing through the second main shock's epicenter; this shows that the second main shock hypocenter is placed in increased (positive) stress region, evidencing the triggering of second main shock due to first main shock (Fig. 7b). Both the second main shock's epicenter and hypocenter are located in areas of positive or increased Coulomb stress change imparted by either the first main shock on second main shock fault (Fig. 7a and b). By considering apparent friction coefficient as $\mu' = 0.4$ (Fig. 7), the coseismic Coulomb failure stress change on the slip direction of the second main shock increased by 0.866 bar. The stress change exceeded the earthquake triggering threshold of 0.1 bar, implying an apparent triggering effect.

However, both main shocks were followed by a number of aftershocks during the period December 20, 2010–April 6, 2011. The epicentral distribution of the aftershocks suggests that the causative faults of the first main shock is aligned in a NE-SW direction and second main shock is aligned in a NW-SE direction, which were activated during the seismic activity. The coseismic Coulomb stress changes due to the both main shocks were calculated to analyze the correlation between increased Coulomb stress regions and locations of aftershock activity. The computation of Coulomb stress field for depth range 0–30 km (Fig. 8) was performed for $\mu' = 0.4$. The coseismic Coulomb stress changes were resolved on optimally-oriented planes of strike-slip faults. To see the overall spatial relationship between Coulomb stress change and aftershock distribution, aftershocks were overlain onto the Coulomb stress change fields. Correlation is strong between increased Coulomb stress region and locations of observed aftershocks as more than 90% of the total aftershocks occurred in the increased zone. Most of the Rigan aftershocks occur in enhanced Coulomb stress regions suggesting that these shocks were triggered due to a transfer of positive Coulomb stress by main shocks. Freed (2005) states the best correlation between increased Coulomb stress and locations of aftershocks is observed at distances larger than a few kilometers from the fault rupture. The slip distribution and rupture geometry influence the near-fault stress changes. The occurrence of aftershock activity in stress shadow regions is generally due to over simplifications of modeled fault-slip, unaccounted heterogeneity of crust and existence of small faults with different azimuthal orientations. A few aftershocks occurred in the region of decreased Coulomb stress (stress shadow region; Fig. 8). Ideally a few aftershocks or triggered earthquakes should occur in such regions if the Coulomb hypothesis is valid (Harris and Simpson, 1998).

6. Results and Conclusion

Recent years have demonstrated a noteworthy consideration paid to aftershock sequences, since they can help in understanding the mechanism of earthquakes and they are useful resources of data about earthquakes nucleation and the physical properties of materials in fault areas in which slip takes place during an earthquake (Frohlich and Willemann, 1987). Kisslinger and Jones (1991) and Kisslinger (1996) recommended that large amounts of residual seismic energy is generated by heterogeneous materials in the focal region considered is discharged by aftershocks. Statistical properties of aftershocks have been studied for long time (Utsu, 1961, 1969; Utsu et al., 1995; Guo and Ogata, 1999). However, most studies managed only to assess the distribution of aftershocks in time, space and magnitude domains. For this work, aftershock data from IGUT's earthquake catalog the period December 20, 2010 till April 6, 2011 was adopted. Two main aftershock sequences which triggered by two main shocks during the Rigan sequence have been considered; the first sequence which was triggered by an event on December 20, 2010 with magnitude M_N 6.5 and second sequence which triggered by separate event which occurred on January 27, 2011 with magnitude M_N 6.0. The causative fault related with the first and second sequence has a NE–SW and NW-SE strike respectively, as documented by both, spatial aftershock distribution and fault plane solution determined.

The *b*-value of the Gutenberg–Richter frequency magnitude was estimated using the maximum likelihood estimation. To derive dependable *b*-value estimates, only events with magnitude over the threshold magnitude of completeness M_c were chosen. The magnitude above which the total events have been recorded, M_c, is a critical parameter for seismicity-based investigations since it is important to utilize the maximum number of events to determine such seismic hazard values, which drives regularly to underestimation of M_c (Wiemer and Wyss, 2000). As shown in Fig. 4, M_c was equal to 3.2 for both sequences, and the *b*-value was calculated equal to b = 0.89±0.08 and b = 0.88±0.08 for the first sequence and second sequence respectively. The processed *b*-values are smaller than the worldwide mean estimation of 1.0 which is associated with a low degree of heterogeneity, large velocity of deformation and large faults (Manakou and Tsapanos, 2000). The low *b*-value is additionally synonymous to the occurrence of larger size aftershocks that are affected because of the attendance of giant size asperities in the rupture zone. The estimated low *b*-value for these main shocks sequences drives that the region is indicated by large differential stress and the genesis of giant aftershock activity in a short time interval gives power this.

The significant change among the magnitudes of the main shock and the biggest aftershock relies on the stress situation and heterogeneity of the rock mass. Based on Bath’s law

(Bath, 1965), the distinction between the size of the main shock and the biggest aftershock of an earthquake sequence has a steady statistical mean value of 1.2, and is outwardly independent of the magnitude of the main shock. It infers that the strain transfer chargeable for the incidence of aftershocks is a self-similar process (Shcherbakov and Turcotte, 2004). However, the relationship among magnitude of the main shock and its biggest aftershock for both sequences has been studied on the basis of modified Bath's law. The magnitude difference (Δm) is found to be 1.4 and 0.7 for first and second sequence respectively. So that both sequences do not pursue the Bath's law. Similar characteristics are also reported by many previous authors (e.g Papazachos et al., 1967; Shcherbakov et al., 2005; Hamdache et al. , 2013). Taking after Shcherbakov and Turcotte (2004), Bath's law and the Gutenberg–Richter relationship are consolidated keeping in mind the end goal of determining the biggest aftershocks (m^*) which can happen in each sequence. This m^* is directly associated to the parameter *a* and *b* of the Gutenberg–Richter by the relation $a = bm^*$. The independence of the fraction of the elastic energy which expands the stress in contiguous rock, on the size of earthquake clarifies the legitimacy of Bath law in its unique and modified model (Shcherbakov and Turcotte, 2004). However, Shcherbakov and Turcotte (2004) concluded that all the aftershocks play a similar role in relaxing the stress transferred by the main shock. The partitioning of energy requires that an expansive division of collected energy is discharged in the main shock and just a moderately little part of the energy discharged in the aftershock succession. Therefore, by taking a = 4.77 and b = 0.89 for the first sequence and a = 4.86 and b = 0.88 for the second sequence the modified magnitude of biggest aftershock (M^*) as 5.3 and 5.5 for first and second sequences respectively. Moreover, magnitude differences ($\boldsymbol{\Delta} m^*$) as 1.2 and 0.5 for first and second sequences have been calculated respectively. However, 2.2% of all energy is related with aftershock activity while 97.8% is associated with main shock in the first sequence. In comparison, 20% of the total energy is associated with aftershock activity while 80% is associated with main shock for the second sequence. In any case, The power content of the aftershock sequence is increasing with lowering Δm.

The temporal decay of aftershocks pattern has been evaluated using the modified Omori law (Utsu et al., 1995). In keeping with Olssen (1999) and Utsu et al. (1995), *p*-values usually range between 0.5 and 1.8, and this parameter differs from sequence to sequence based on tectonic situation in the considered area. However, it is not clear which factor impact most on calculated *p*- values. More consideration is paid in the estimation of the *p*-value utilizing the maximum likelihood as explained by Nyffengger and Frolich (1998, 2000). The *p*-value equal to 1.1 ± 0.12 and 1.1 ± 0.1 were obtained for first and second sequences respectively. The *p*-value is larger than the mean value (1.0) in the both sequence. The higher *p*-value infers faster decay of aftershock activity. However, the *p*-value approaching a value of 1.0 pronounces that earthquake happened in an tectonically active region with an amount of stress dissipation.

A natural way to analyze the spatial distribution of seismicity is to determine the so called fractal dimension (D_c-value). In particular, fault networks and epicenter distributions have fractal properties (Goltz, 1998). It is well identified that earthquakes cluster both in time and space, either on a long-term (Kagan and Jackson, 1991) or in the short-term time scale (foreshocks and aftershocks). For evaluating fractal dimension values, the correlation dimension approach was adopted, which is seen to be a more robust means for point process interrogation. Be that as it may, the variety in fractal measurement zones gives a lot of information about the geological heterogeneity and constancy of the region (Dimitriu et al., 1993; DeRubeis et al., 1993). Moreover, value of D_c near to zero may be interpreted as being all events bunched into one point, near to 1.0 indicates dominance of the sources, near to 2.0 indicates the planar fractures surface being filled up and a value near to 3.0 indicates that earthquake fractures are topping off a crustal volume. In this research, the spatial fractal dimension was evaluated from the double-logarithmic plot of the correlation integral and distance between hypocenters, and found equal to 2.34 ± 0.03 and 2.54 ± 0.02 for the first and second sequences respectively (Fig. 6). A D_c-value higher than 2.0 reveals that the earthquakes are haphazardly distributed in the fault zone crustal volume.

There are numerous studies attempting to understand earthquake interactions that have concentrated on the hypothesis of static stress transfer as a possible triggering mechanism. Calculation of static Coulomb strain can assist our understanding to comprehend stress interaction process and to provide an explanation for the evolution of seismicity patterns (e.g., Harris, 1998; Stein, 1999). The Coulomb stress change due to the first main shock which occurred on December 20, 2010 with magnitude of M_N 6.5 (Global CMT M_w 6.5) was calculated and examined in relation to its probable interaction with the second main shock which occurred on January 27, 2011 with magnitude of M_N 6.0 (Global CMT M_w 6.2). The Coulomb stress change indicates that the epicenter of second main shock located in the positive (increased) Coulomb stress lobe. Moreover, the cross-sectional and map views of the Coulomb stress change due to the first main shock indicates that the second main shock lies in the increased (positive) Coulomb stress lobe. Moreover, the second main shock was calculated to receive approximately 0.866 bar. It is clear that the Coulomb stress change surpassed the triggering threshold of 0.1 bar which reveals that the second main shock was triggered by the transfer of positive Coulomb stress due to a first main shock. coseismic Coulomb stress modeling was performed for both main shocks. The assemblage between aftershock distribution and increased Coulomb stress region indicates that more than 90% aftershocks have been triggered by transfer of positive Coulomb stress due to coseismic slip of these main shocks. The correspondence between aftershock activity and the positive Coulomb failure stress regions produced by these main shocks are in good agreement with previous studies that provide a possible explanation of aftershock triggering in this situation (King et al., 1994; Stein et al., 1994; Harris, 1998; Toda et al., 1998; Karakostas et al., 2003, 2004; Rajput et al., 2005; Gahalaut, 2008; Bayrak et al., 2013).

Acknowledgments

The authors would like to thank the Institute of Geophysics at University of Tehran (IGUT) for providing their data for analysis. The Computer programs, Coulomb 3.3 (Toda et al. 2011) and Zmap (Wiemer, 2001) were also used.

References

Ambraseys, N N., Melville, C P., 1982. A History of Persian Earthquakes, Cambridge University Press, Cambridge.

Ashtari-Jafari, M,. 2011. Teleseismic source parameters of the Rigan county earthquakes and evidence for a new earthquake fault, Pure Appl. Geophys. 169, 1655–1661, doi: 10.1007/s00024-011-0433-9.

Bayrak, Y.,, Yadav, R B S., Kalafat, D., Tsapanos, T M., Çınar, H., Singh, A P,. Bayrak, E,. Yılmaz, Ş., Öcal, F., Koravos, G., 2013. Seismogenesis and earthquake triggering during the Van (Turkey) 2011 seismic sequence. Tectonophysics, 601 (2013) 163–176.

Bath, M., 1965. Lateral inhomogeneties in the upper mantle. Tectonophysics 2, 483– 514.

Ben-Zion, Y., 2008. Collective behavior of earthquakes and faults: Continuum-discrete transitions, progressive evolutionary changes, and different dynamic regimes. Rev Geophys 46: RG4006.i:10.1029/2008rg000260.

Berberian, M., 1976. Contribution to the Seismotectonics of Iran (Part II)". Geological Survey of Iran, Report No. 39, p. 517.

Berberian, M., 1995. Natural hazards and the first earthquake catalogue of Iran, historical hazards in Iran prior to 1900. A UNESCO/IIEES Publication During UN/ IDNDR IIEES, Iran.

Bowman, J. R., 1997. A seismicity precursor to a sequence of Ms 6.3-6.7 midplate earthquakes in Australia, Pure Appl. Geophys., *149*, 61-78.

Chan, C H., Wu, Y M., 2014. Seismic behavior in central Taiwan: response to stress evolution following the 1999 Mw 7.6 Chi-Chi earthquake. J. Asian Earth Sci. 90, 101–105.

Chen, L W., Zhang, P Z., Lu,Y Z., 2008. Numerical simulation of loading/ uploading effect on Coulomb Failure stress among strong earthquakes in Sichuan-Yunnan area. Chin. J. Geophys. 51 (5), 1411–1421.

Console, R., Lombardi, A M., Murru, M., Rhodes, R., 2003. Bath's law and the selfsimilarity. J. Geophys. Res. 108, 2128.

Deng, J., Sykes, L R., 1997. Evolution of the stress field in Southern California and triggering of moderate-size earthquakes: a 200-year perspective. J. Geophys. Res. 102 (B5), 9859–9886.

DeRubeis, V., Dimitriu, P., Papadimitriou, E., Tosi, P., 1993. Recurrent patterns in the spatial behavior of Italian seismicity revealed by the fractal approach. Geophys Res Letts 20/18, 1911–1914.

Dimitriu, P P., Papadimitriou, E E., Papazachos, B C., Tsapanos, T M., 1993. Global study of the distribution of earthquakes in space and in time by the fractal method. In: Proc. 2nd Cong. Hellenic Geophys. Union, Florina, May 5–8, 1993, vol. 1, pp. 164–174.

Freed, AM., 2005. Earthquake triggering by static, dynamic, and postseismic stress transfer. Ann Rev Earth and Planetary Sci 33, 335–367.

Frohlich, C., Willemann , R., 1987 .Statistical methods for comparing directions to the orientations of focal mechanisms and wadati-beniof zones. Bull. Seismol. Soc. Am. 77 (6), 2135–2142.

Gahalaut, V K., 2008. Coulomb stress change due to 2005 Kashmir earthquake and implications for future seismic hazards. J Seismol 12, 387–394.

Gkarlaouni, Ch., Papadimitriou, E E., Karakostas, V G., 2008. Implication of fault interaction to seismic hazard assessment in Sichuan-Yunnan provinces of southeastern China. Acta Seismol. Sin. 21 (2), 181–201.

Goltz, C., 1998. Fractal and chaotic properties of earthquake, in Lecture Notes in Earth Sciences, Springer, New York, 175 pp.

Grassberger, P., Procaccia, I., 1983. Measuring the strangeness of strange attractors. Physics D 9, 189–208.

Guo, Z., Ogata, Y., 1999. Statistical relation between the parameters of aftershocks in time, space and magnitude. J. Gophys. Res. 102 (B2), 2857–2873.

Gutenberg, B., Richter, C.F., 1944. Frequency of earthquakes in California. Bulletin of the Seismological Society of America 34, 185–188.

Hamdache, M., Pelaez, J A., Talbi, A., 2013. Analysis of aftershock sequences in South and Southeastern Spain. Phyics and Chemist of the Earth 63 (2013) 55–76.

Han, Z J., Dong, S P., Xie, F R., 2008. Earthquake triggering by static stress: the 5 major earthquakes with MP7 (1561–1920) in the northern section of south– north seismic zone, China. Chin. J. Geophys. 51 (6), 1776–1784.

Hardebeck, J L., Nazareth, J J., Hauksson, E., 1998. The static stress change triggering model: Constraints from two southern California aftershocks sequences. J Geophys Res. 103, 24,427–24,437.

Harris, R A., 1998. Introduction to special section: stress triggers, stress shadows and implications for seismic hazard. J Geophys Res 103 (10), 24347–24358.

Harris, R., Simpson, RW., 1988. Suppression of large earthquakes by stress shadows: a comparison of Coulomb and rate-state failure. J Geophys Res 103:24439–24451.

He, J K., Xia ,W H., Lu, S J., 2011. Three-dimensional finite element modeling of stress evolution around the Xiaojiang fault system in the southeastern Tibetan plateau during the past _500 years. Tectonophysics 507, 70–85.

He, P., Wen, Y M., Xu, C J., 2013. The large aftershocks triggered by the 2011 Mw9.0 Tohoku-Oki earthquake, Japan. J. Asian Earth Sci. 74, 1–10.

Hessami, KH., Jamali, F., 2006. Explanatory notes to the map of major active faults of Iran. J Seismol Earthq Eng 8(1):1–11.

Hirata, T., 1989. A correlation between the b-value and the fractal dimension of earthquakes. J. Geophys. Res. 94, 7507–7514.

Kagan, Y Y., Jackson, D D., 1991. Long term earthquake clustering: J Geophys Res , 104, 117-133.

Karakostas, V G., Papadimitriou, E E., Karakaisis, G F., Papazachos, C B., Scordilis, E M., Vargemezis, G., Aidona., E., 2003. The 2001 Skyros, Northern Aegean, Greece, earthquake sequence: off-fault aftershocks, tectonic implications and seismicity triggering. Geophys Res Letts, Vol 30, Issue 1, Pages 12-1–12-4.

Karakostas, V G., Papadimitriou, E E., Papazachos, C B., 2004. Properties of the 2003 Lefkada Ionian Islands, Greece, earthquake seismic sequence and seismicity triggering. Bull Seismol Soc Am 94, 1976–1981.

Karakostas, V., Papadimitriou, E., Jin, X S,. 2013. Potential of future seismogenesis in Hebei Province (NE China) due to stress interactions between strong earthquakes. J. Asian Earth Sci. 75, 1–12.

King, G.C.P., Cocco, M., 2000. Fault interactions by elastic stress changes: new clues from earthquake sequences. Advances in Geophysics 44, 1–38.

King, G C P., Stein, R S., Lin, J., 1994. Static stress changes and the triggering of earthquakes. Bull Seismol Soc Am 84, 935–993.

Kisslinger, C., Jones, L M., 1991. Proprieties of aftershocks in Southern California. J. Geophys. Res. 103 (24), 453-24,465.

Kisslinger, C., 1996. Aftershocks and fault-zone properties. Adv. Geophys. 18, 1–36.

Kisslinger, C., Jones, L. M., 1991. Proprieties of aftershocks in Southern California. J. Geophys. Res. 103 (24), 453-24,465.

Li, Y J., Chen, L W., Lu, Y Z., 2013. Numerical simulation on influences of Wenchuan earthquake on the stability of faults in the neighborhood. Earth Sci. 38 (2), 398–410.

Lin, J., Stein, R S., 2004. Stress triggering in thrust and subduction earthquakes and stress interaction between the southern San Andreas and nearby thrust and strike-slip faults, J. Geophys. Res., 109, B02303.

Liu. M., Yang, Y., Shen, Z K., 2007. Active Tectonics and Intracontinental Earthquakes in China: The Kinematics and Geodynamics. Geological Society of America, Special Paper 425, pp. 299–318.

Manakou, M V., Tsapanos, T M. 2000. Seismicity and seismic hazard parameters evaluation in the island of Crete and the surrounding area inferred from mixed data files, Tectonophysics. 321: 157–178.

Mendoza, C., Hartzell, S H., 1988). Aftershock patterns and main shock faulting. Bull. Seismol Soc Am. 78, 1438-1449.

Meyer, B., LeDortz K., 2007. Strike-slip kinematics in Central and Eastern Iran: estimating fault slip-rates averaged over the Holocene, Tectonics, Vol 26, Issue 5.

Nalbant, S S., Hubert. A., King, G C P., 1998. Stress coupling between earthquakes in northwest Turkey and the north Aegean Sea. J Geophys Res 103, 24,469–24,486.

Narteau, C., Byrdina, S., Shebalin, P., Schorlemmer, D,. 2009. Common dependence on stress for the two fundamental laws of statistical seismology. Nature, 462/3 December 2009.

Nuttli, O W., 1973. Seismic wave attenuation relations for eastern North America. J Geophys Res 78, 855–876.

Nyffengger, P., Frolich, C., 1998. Recommandations for determining p values for aftershock sequence and catalogs. Bull. Seismol. Soc. Am. 88 (5), 1144–1154.

Nyffengger, P., Frolich, C., 2000. Aftershock occurrence rate decay properties for intermediate and deep earthquake sequences. Geophys. Res. Lett. 27 (8), 1215– 1218.

Ogata, Y., Imoto, M., Katsura, K., 1991. 3-D spatial variation of b-values of magnitude–frequency distribution beneath the Kanto District, Japan. Geophys. J. Int. 104 (1), 135–146.

Ogata, Y., Katsura, K., 1993. Analysis of temporal and spatial heterogeneity of magnitude frequency distribution inferred from earthquake catalogs, Geophys. J. Int., 113, 727–738.

Okada, Y., 1992. Internal deformation due to shear and tensile faults in a half-space. Bull Seismol Soc Am 82, 1018–1040.

Olssen, R., 1999. An estimation of the maximum b values in the Gutenberg–Richter relation. Geodynamics 27, 547–552.

Papazachos, B C., Delibasis, N., Liapis, N., Moumoulidis, G., Purcaru, G., 1967. Aftershock sequences of some large earthquakes in the region of Greece. Ann. Geofis. 20, 1–93.

Papadimitriou, E E., Sykes, L R., 2001. Evolution of stress field in the Northern Aegean Sea (Greece). Geophys J Int 146, 747–759.

Papadimitriou, E E., Wen, X Z., Karakostas, V G., 2004. Earthquake triggering along the Xianshuihe fault zone of western Sichuan, China. Pure Appl Geophys.161, 1683–1707.

Papadimitriou, E. E., Garlaouni, Ch. G, Jin, X S., 2007. Application of the stress evolutionary model along the Xiaojiang fault zone in Yunnan Province, Southeast China. Acta Geophys. 55 (4), 577–593.

Parsons, T., Stein, R S., Simpson, R W., 1999. Stress sensitivity of fault seismicity: a comparison between limited-offset oblique and major strike-slip faults. J Geophys Res 104, 20,183–20,202.

Parsons, T., Chen, J., Kirby, E., 2008 Stress changes from the 2008 Wenchuan earthquake and increase hazard in the Sichuan basin. Nature 454, 509–510.

Qian, Q., Han, Z J., 2013. Influence of the 2008 Wenchuan earthquake (Mw7.9) on the occurrence probability of future earthquakes on neighboring faults. J. Asia Earth Sci. 70–71, 283–294.

Rajput, S., Gahalaut,. Sahu, V K ., 2005. Coulomb stress changes and aftershocks of recent Indian earthquakes. Current Science 88 (6), 576–588.

Rezapour, M., Mohsenpur, A., 2013. The 2010 Mw 6.5 Rigan, Iran, Earthquake Aftershock Sequence, Bull Seismological Soc Am, Vol. 103, No. 3, pp. 1793-1800.

Rybicki, K., 1973. Analysis of aftershocks on the basis of dislocation theory, Phys. Earth Planet. Inter. 7, 409-422.

Sarkar, I., Chander, R., 2003. Role of static stress transfer in earthquake occurrence in the Himalaya. J. Asian Earth Sci. 22 (1), 59–65.

Scholz, C., 1968. Microfracturing and the inelastic deformation of rock in compression. J. Geophys. Res. 73 (4), 1417–1432.

Schorlemmer, D., Wiemer, S., Wyss, M., 2005. Variations in earthquake-size distribution across different stress regimes. Nature 437 (7058), 539–542.

Shcherbakov, R., Turcotte, D L., 2004. A modified form of Bath's law. Bull. Seismol. Soc. Am. 94, 1968–1975.

Shcherbakov, R., Turcotte, D L., Rundle, J E., 2005. Aftershocks statistics. Pure Appl. Geophys. 162, 1051–1076.

Shen, Z K., Wan, Y G., Gan, W J. 2003. Viscoelastic triggering among large earthquakes along the eastern Kunlun fault system. Chinese J Geophys 46 (6), 786–795.

Stein. R S., 1999. The role of stress transfer in earthquake occurrence. Nature 402, 605–609

Stein, R S., Lisowski, M., 1983. The 1979 Homestead Valley earthquake sequence, California: control of aftershocks and postseismic deformation. J. Geophys. Res. Volume 88, Issue Pages 6477–6490.

Stein, R S., King, G C P., Lin, J., 1994. Stress triggering of the 1994 M=6.7 Northridge, California, earthquake by its predecessors. Science 265 (5177), 1432–1435.

Stein, S., Wysession, M., 2002. An Introduction to Seismology, Earthquakes and Earth Structure. Blackwell Publishing Press, UK.

Toda, S., Stein, R S., Reasenberg, P A., Dieterich, J H., 1998 Stress transferred by the Mw = 6.5 Kobe, Japan, shock: effect on aftershocks and future earthquake probabilities. J Geophys Res, Volume 103, Issue 10.

Toda, S., Stein, R., Richards-Dinger, K., Bozkurt, S., 2005. Forecasting the evolution of seismicity in southern California: Animations built on earthquake stress transfer, J. Geophys. Res., Volume 110, Issue 5.

Toda, S., Lin, J., Meghraoui, M., 2008. 12 May 2008 M = 7.9 Wenchuan, China, earthquake calculated to increase failure stress and seismicity rate on three major fault systems. Geophys. Res. Lett. Volume 35, Issue 17.

Toda, S., Stein, R S., Sevilgen, V., Lin, J., 2011. Coulomb 3.3 graphicrich deformation and stress-change software for earthquake, tectonic, and volcano research and teaching-user guide. U.S. Geological Survey Open-File Report 2011-1060.

Turcotte, D., 1997. Fractals and Chaos in Geology and Geophysics. Cambridge University Press, New York, 416 pp.

Urbancic, T., Trifu, C., Long, J., Young, R., 1992. Space–time correlations of b values with stress release. Pure Appl. Geophys. 139 (3), 449–462.

Utsu, T., 1961. A statistical study on the occurrence of aftershocks. Geophysics 30, 521–605.

Utsu, T., 1965. A method for determining the value of b in a formula logN = a – bM showing the magnitude frequency for earthquakes. Geophysical Bulletin Hokkaido University 13, 99–103.

Utsu, T., 1969. Aftershocks and earhquake statistics (I) – some parameters which characterize an Aftershock Sequence and their Interaction. J. Fac. Sci. Hokaido, Univ. Ser. VII (Geophys.) 3, 129–195.

Utsu, T., 2002. A statistical study of occurrence of aftershocks. Geophys. Mag. 30, 521–605.

Utsu, T., Ogata, Y., Matsöra, R S., 1995. The centenary of the Omori formula for a decay law of aftershock activity. J. Phys. Earth 43, 1–33.

Vere-Jones, D., 1969. A note on the statistical interpretation of Bath's law. Bull. Seismol. Soc. Am. 69 (4), 1535–1541.

Vere-Jones, D., Murakami, J., Christophersen, A., 2005. A further note on Bath's law. In: The 4th International Workshop on Statistical Seismology, Tokyo, Japan.

Walker, R T., 2006. A remote sensing study of active folding and faulting in southern Kerman province, S.E. Iran. J. of Struct.Geol., 28, 654–668

Walker, R., Jackson, J. 2004. Active tectonics and late Cenozoic strain distribution in central and eastern Iran, Tectonics, 23, Volume 23, Issue 5 October 2004.

Walker, R T., Bergman, E A., Elliott, J R., Fielding, E J., Ghods, A R., Gorashi, M., Jackson, J., Nazari, H., Nemati, M., Oveisi, B., 2013. The 2010–2011 south Rigan (Baluchestan) earthquake sequence and its implications for distributed deformation and earthquake hazard in southeast Iran, Geophys. J. Int. 193, 349–374.

Wan, Y G., Shen, Z K., Sheng, S. Z,. 2010. The Mechanical effects of the 2008 Ms7.3 Yutian, Xinjiang earthquake on the neighboring faults and its tectonic origin of normal faulting mechanism. Chin. J. Geophys. 53 (2), 280–289. Volume 54, Issue 6 November 2011, Pages 757–765.

Wiemer, S., 2001. A software package to analyze seismicity: ZMAP. Seismol Res Letts 72, 373–382.

Wiemer, S., Wyss, M., 2000. Minimum magnitude of completness in earthquake catalogs: Examples from Alaska, the Western United States, and Japan. Bull. Seismol. Soc. Am. 90, 859–869.

Yamakawa, N., 1968. Foreshocks, aftershocks and earthquake swarms (IV) – frequency decrease of aftershocks in its initial and later stages. Papers in Meteorology and Geophysics 19, 109–119.

Figure Captions

Fig.1. Simplified tectonic map of SW Iran (Black Stars show epicenter of main shock which occurred December 20,2010 and January 27, 2011, Blue Stars show instrumental event and Gray Stars show Historical event and major faults adopted from Ashtari-Jafari (2011)).

Fig.2. Epicentral location of Rigan sequence occurred during the period of December 20, 2010–April 6, 2011. (Frist main shock shown by Red Star, Second main shock shown by Yellow Star).

Fig.3a. Cumulative number of earthquakes with $M_N \geq 2.6$. The Red star is the first main shock M_N = 6.5) and Yellow star is second main shock (M_N = 6.0).**Fig.3b.** Plot of magnitude versus time. **Fig.3c.** spatial distribution of events, which occurred from December 20, 2010 until before Occurrence second main shock (Blue Stars are events with magnitude $M_N \geq 4.0$. **Fig.3d.** spatial distribution of events which occurred from January 27, 2011 till April 6, 2011 (Green Stars are events with magnitude $M_N \geq 4.0$).

Fig. 4. Frequency–magnitude distribution of G–R relationship (logN = a–bM). **a**, First main shock sequence. **b**, second main shock sequence.

Fig. 5. Temporal variations decay of *p*-values for Rigan aftershock sequence. **a**, first main shock sequence. **b**, second main shock sequence.

Fig. 6. Graph which shows the spatial fractal dimension (D_c) of the aftershocks distribution. Solid circles show the data for which best fit was performed for the computation of D_c-value. **a**, First main shock sequence. **b**, second main shock sequence.

Fig.7a. Coseismic Coulomb stress changes (in bars) due to first main shock (M_w 6.5) resolved at depth 14.3 km (depth of the second main shock (M_w 6.2)). **Fig.7a.** the cross-sectional view of Coulomb stress due to first main shock (M_w 6.5) along line AB.

Fig.8. Combined coseismic Coulomb stress changes (in bars) due to the first main shock and second main shock within depth range of 0–30 km. The locations of aftershocks occurred during the period December 20, 2010–April 6, 2011 are shown with green circles. **Fig.**

Fig.1

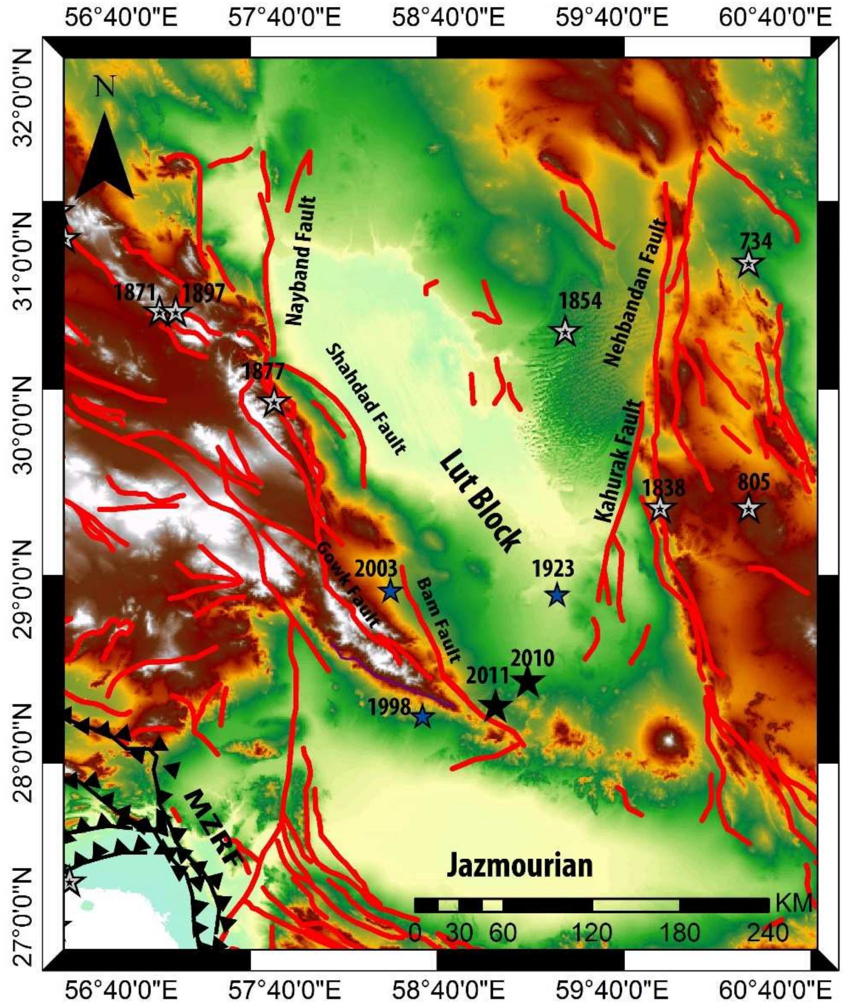
56°40'0"E
57°40'0"E
58°40'0"E
59°40'0"E
60°40'0"E
32°0'0"N
31°0'0"N
30°0'0"N
29°0'0"N
28°0'0"N
27°0'0"N
N
Nayband Fault
Shahdad Fault
Nehbandan Fault
Kahurak Fault
Lut Block
Gowk Fault
Bam Fault
MZRF
Jazmourian
1871
1897
1877
1854
734
1838
805
2003
1923
2010
2011
1998
KM
0 30 60 120 180 240

Fig.2

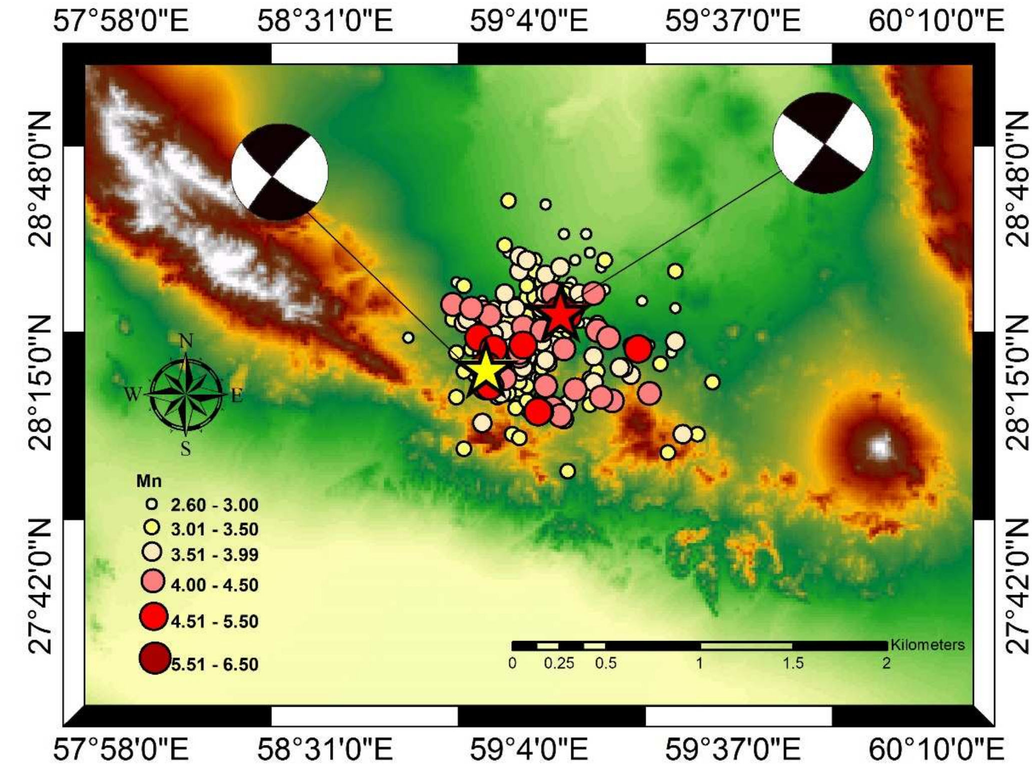
57°58'0"E
58°31'0"E
59°4'0"E
59°37'0"E
60°10'0"E
28°48'0"N
28°15'0"N
27°42'0"N
N
W
E
S
Mn
2.60 - 3.00
3.01 - 3.50
3.51 - 3.99
4.00 - 4.50
4.51 - 5.50
5.51 - 6.50
Kilometers
0
0.25
0.5
1
1.5
2

Fig.3.a

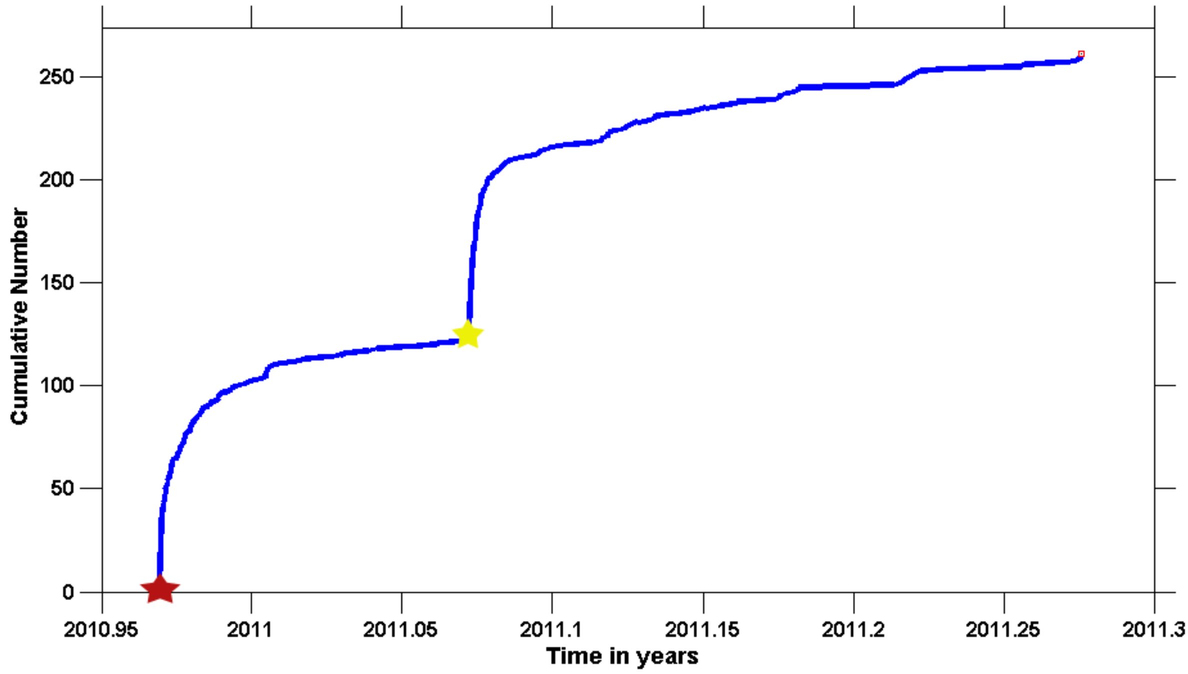

Cumulative Number
250
200
150
100
50
0
2010.95
2011
2011.05
2011.1
2011.15
2011.2
2011.25
2011.3
Time in years

Fig.3.b

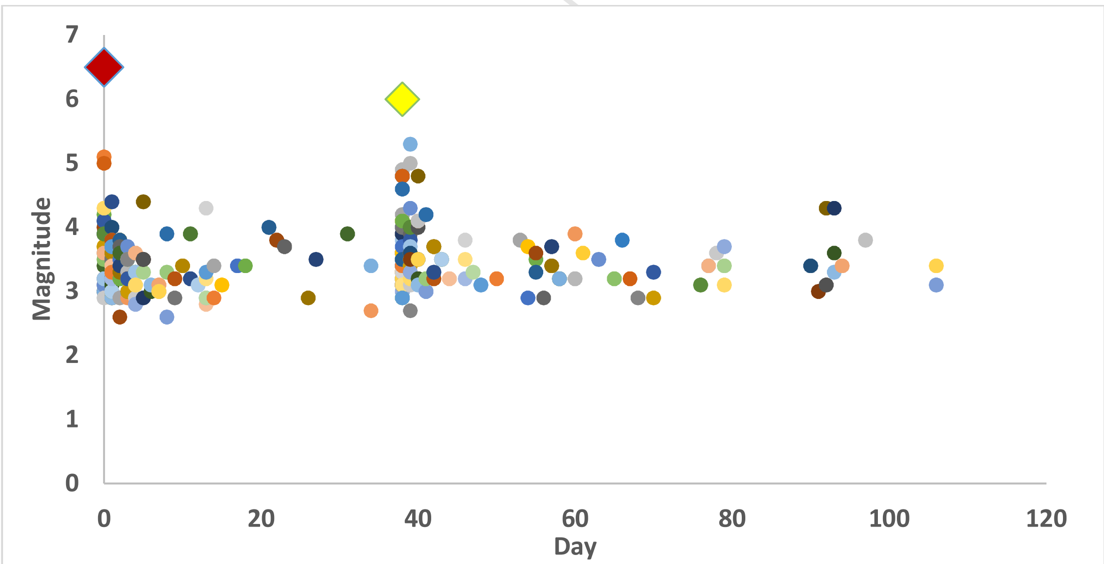

Magnitude
7
6
5
4
3
2
1
0
0
20
40
60
80
100
120
Day

Fig.3c

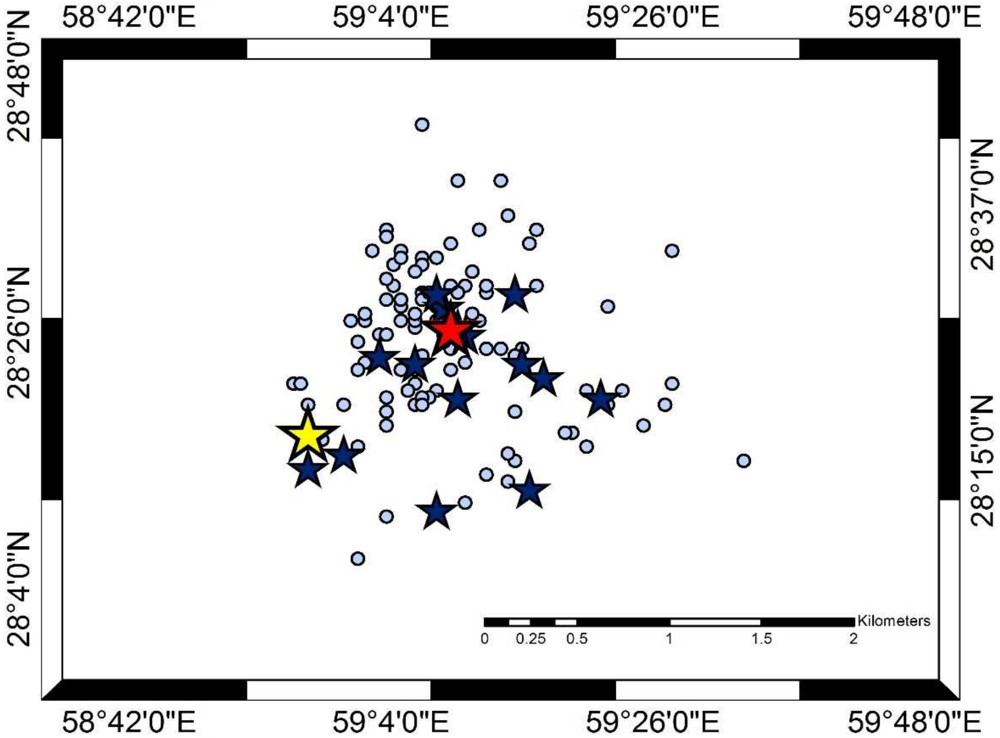
58°42'0"E
59°4'0"E
59°26'0"E
59°48'0"E
28°48'0"N
28°37'0"N
28°26'0"N
28°15'0"N
28°4'0"N
Kilometers
0
0.25
0.5
1
1.5
2

Fig.3d

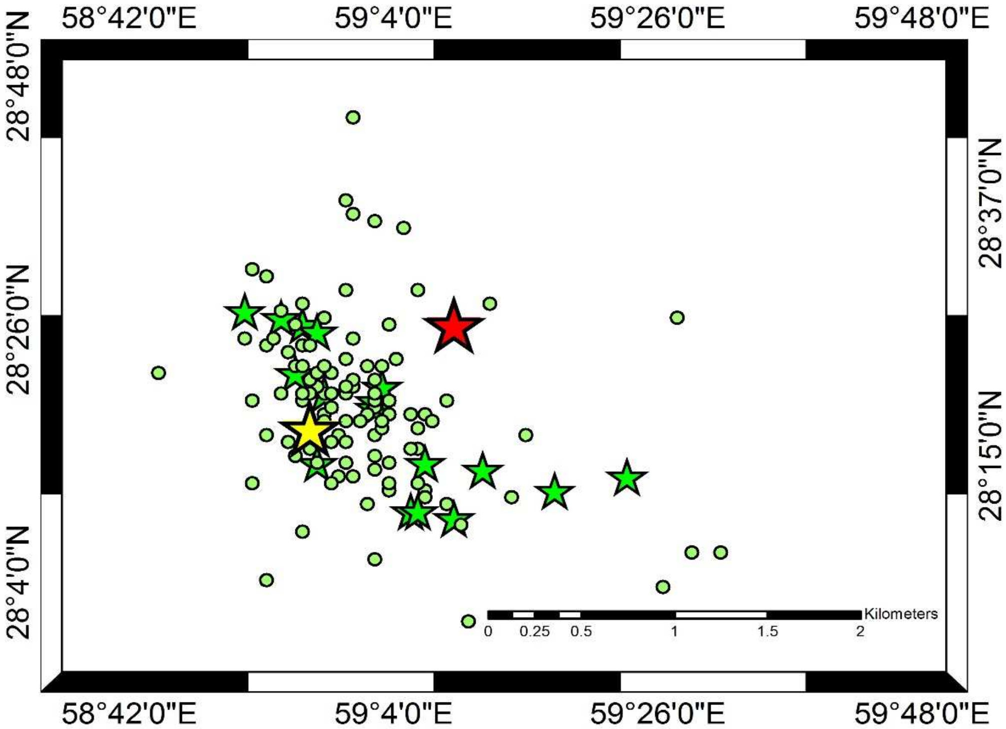
58°42'0"E
59°4'0"E
59°26'0"E
59°48'0"E
28°48'0"N
28°37'0"N
28°26'0"N
28°15'0"N
28°4'0"N
Kilometers
0
0.25
0.5
1
1.5
2

Fig.4a

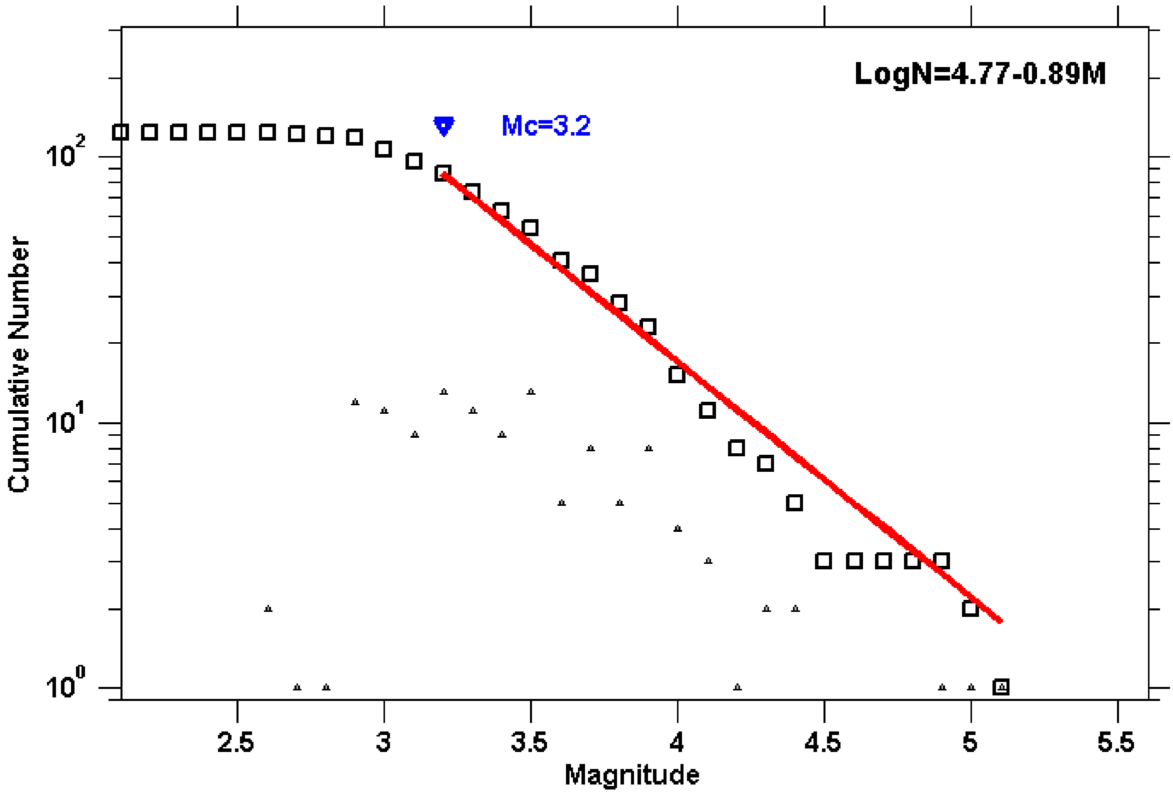

LogN=4.77-0.89M
Mc=3.2
Cumulative Number
Magnitude
10^2
10^1
10^0
2.5
3
3.5
4
4.5
5
5.5

Fig.4b

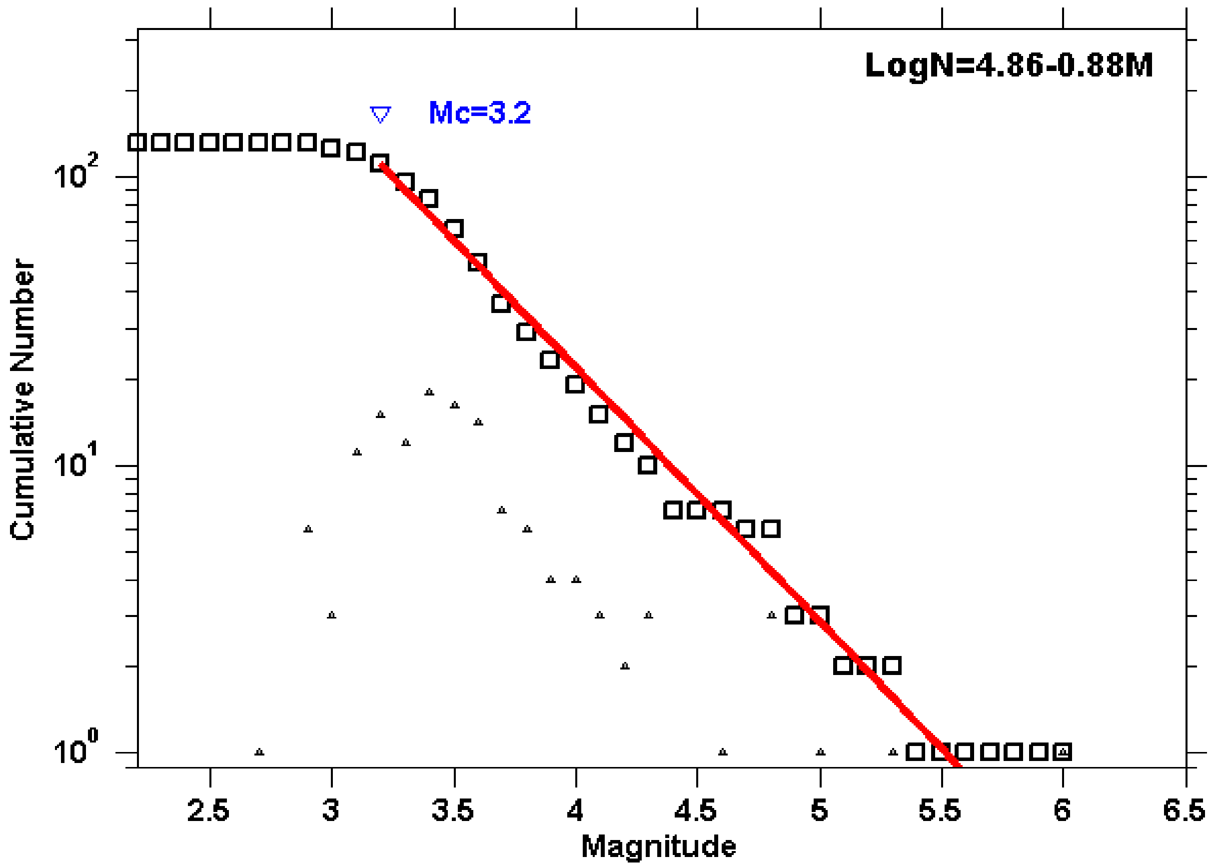

LogN=4.86-0.88M
Mc=3.2
Cumulative Number
Magnitude
10^2
10^1
10^0
2.5
3
3.5
4
4.5
5
5.5
6
6.5

Fig.5a

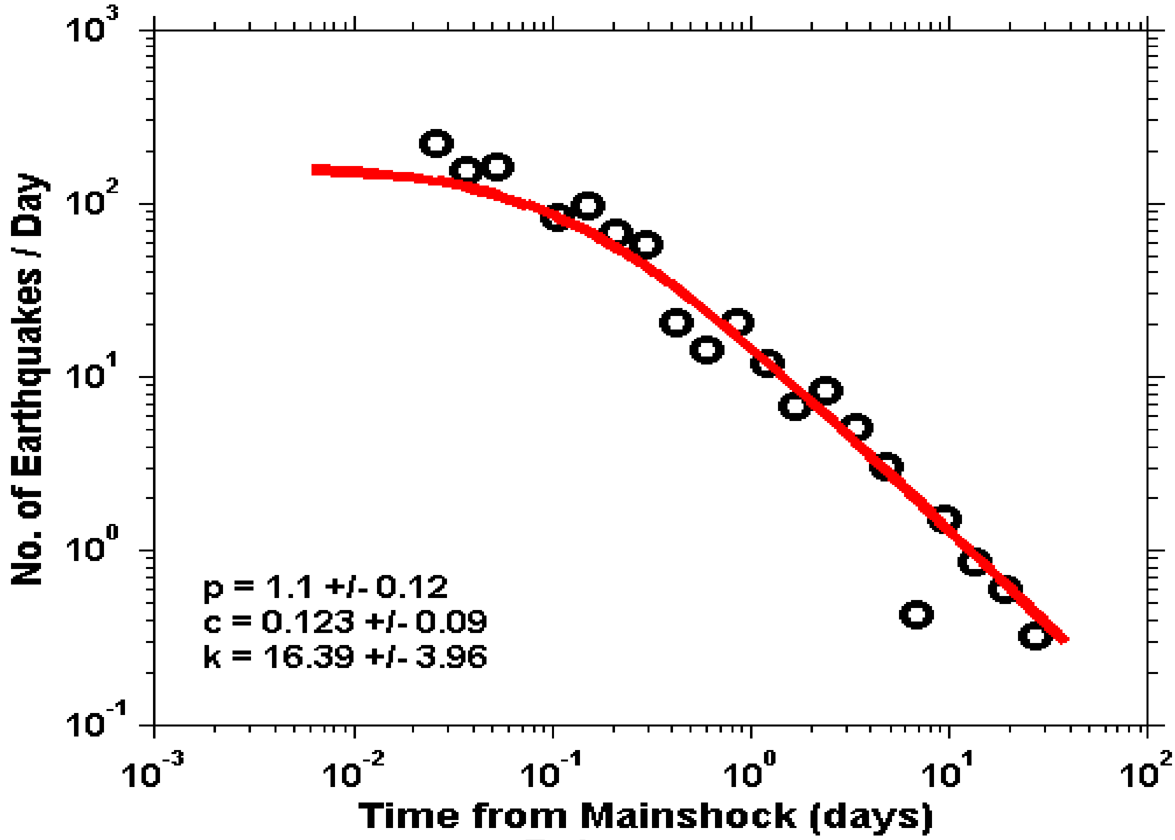
p = 1.1 +/- 0.12
c = 0.123 +/- 0.09
k = 16.39 +/- 3.96
No. of Earthquakes / Day
Time from Mainshock (days)

Fig.5b

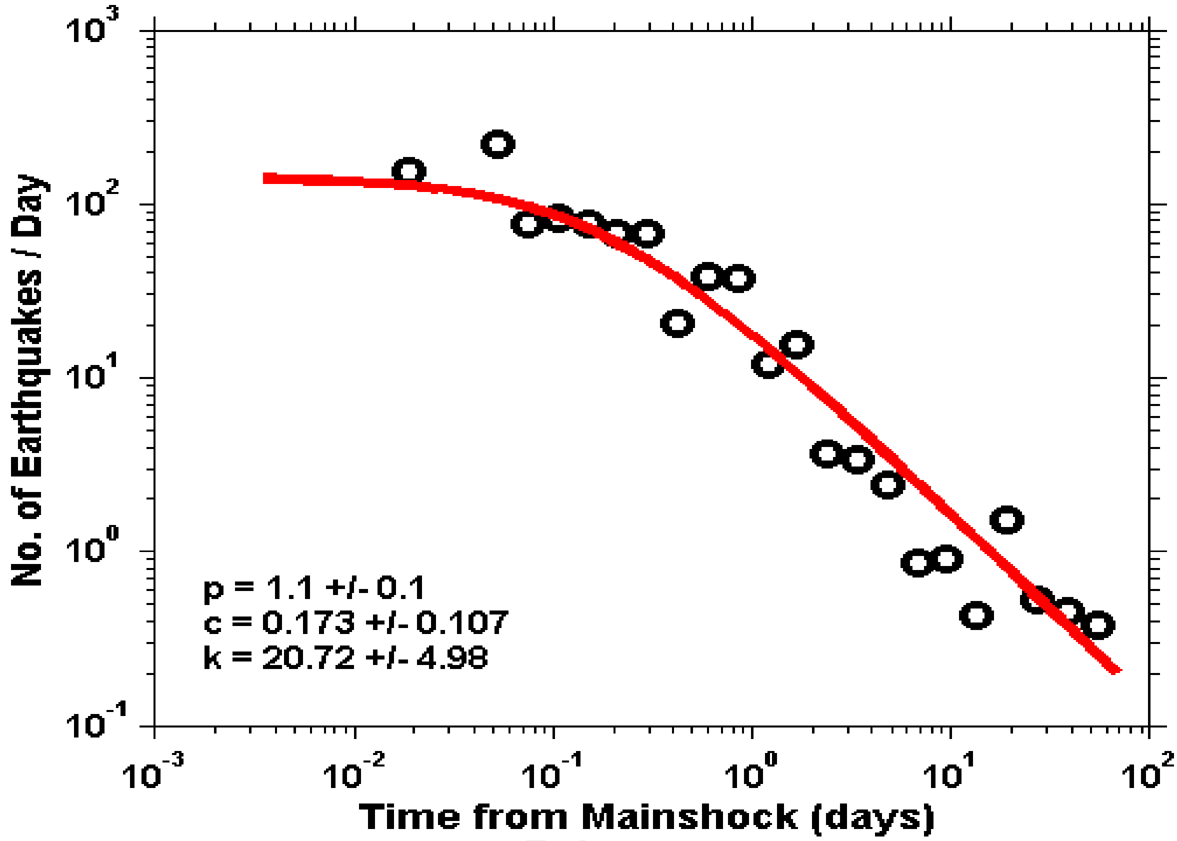

10^3
10^2
10^1
10^0
10^{-1}
No. of Earthquakes / Day
p = 1.1 +/- 0.1
c = 0.173 +/- 0.107
k = 20.72 +/- 4.98
10^{-3}
10^{-2}
10^{-1}
10^0
10^1
10^2
Time from Mainshock (days)

Fig.6a

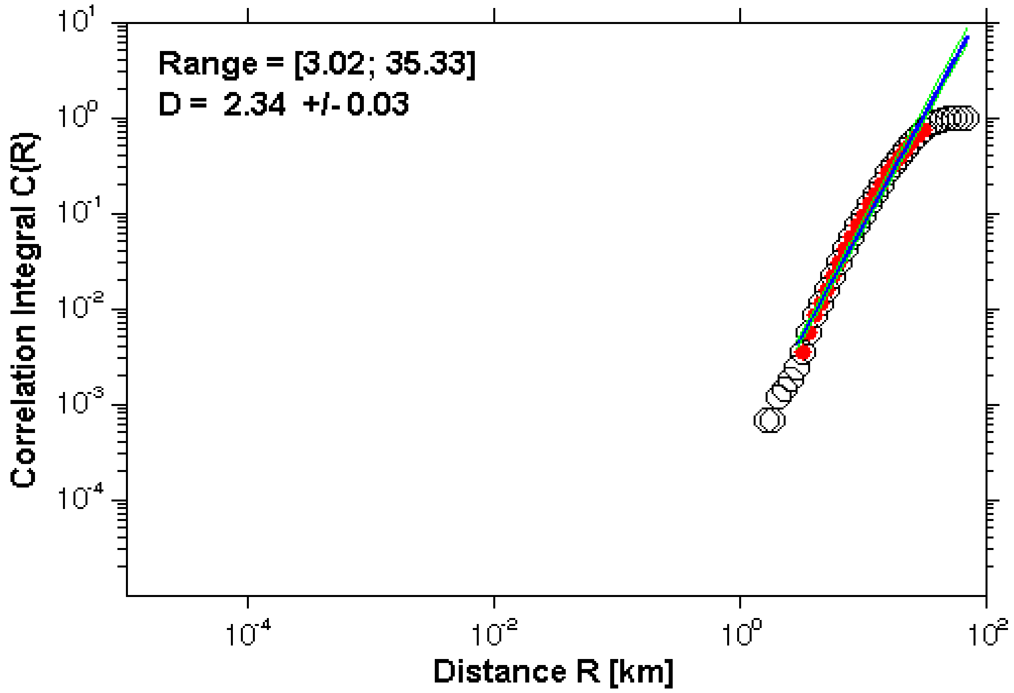
Range = [3.02; 35.33]
D = 2.34 +/- 0.03
Correlation Integral C(R)
Distance R [km]
10¹
10⁰
10⁻¹
10⁻²
10⁻³
10⁻⁴
10⁻⁴
10⁻²
10⁰
10²

Fig.6b

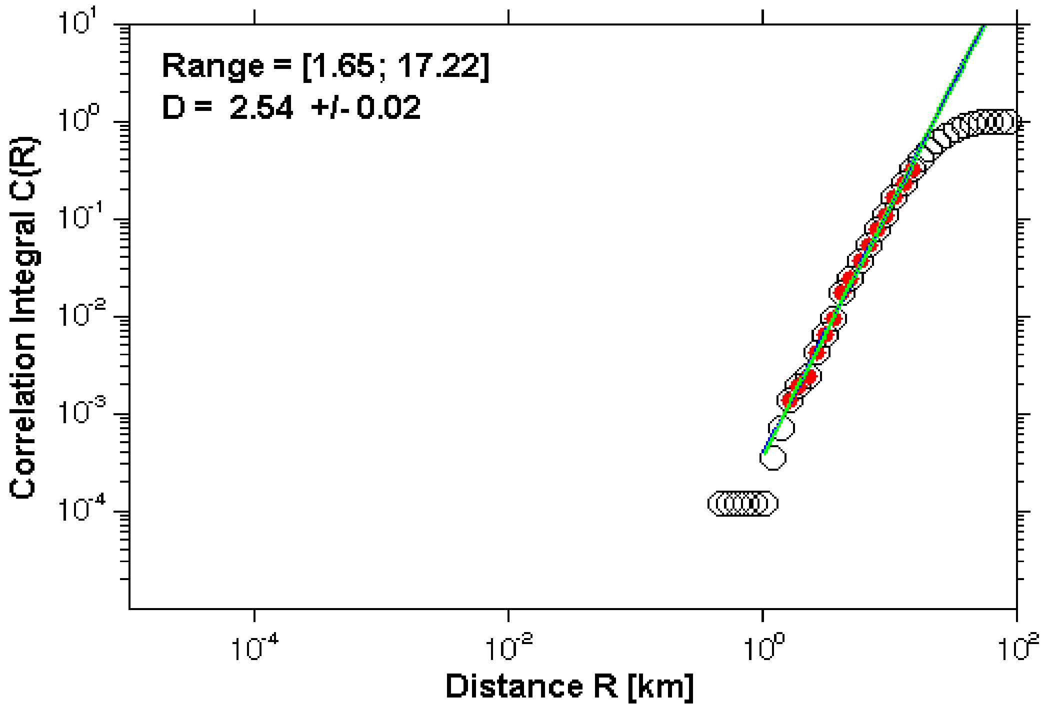
Range = [1.65; 17.22]
D = 2.54 +/- 0.02
Correlation Integral C(R)
Distance R [km]
10¹
10⁰
10⁻¹
10⁻²
10⁻³
10⁻⁴
10⁻⁴
10⁻²
10⁰
10²

Fig.7a

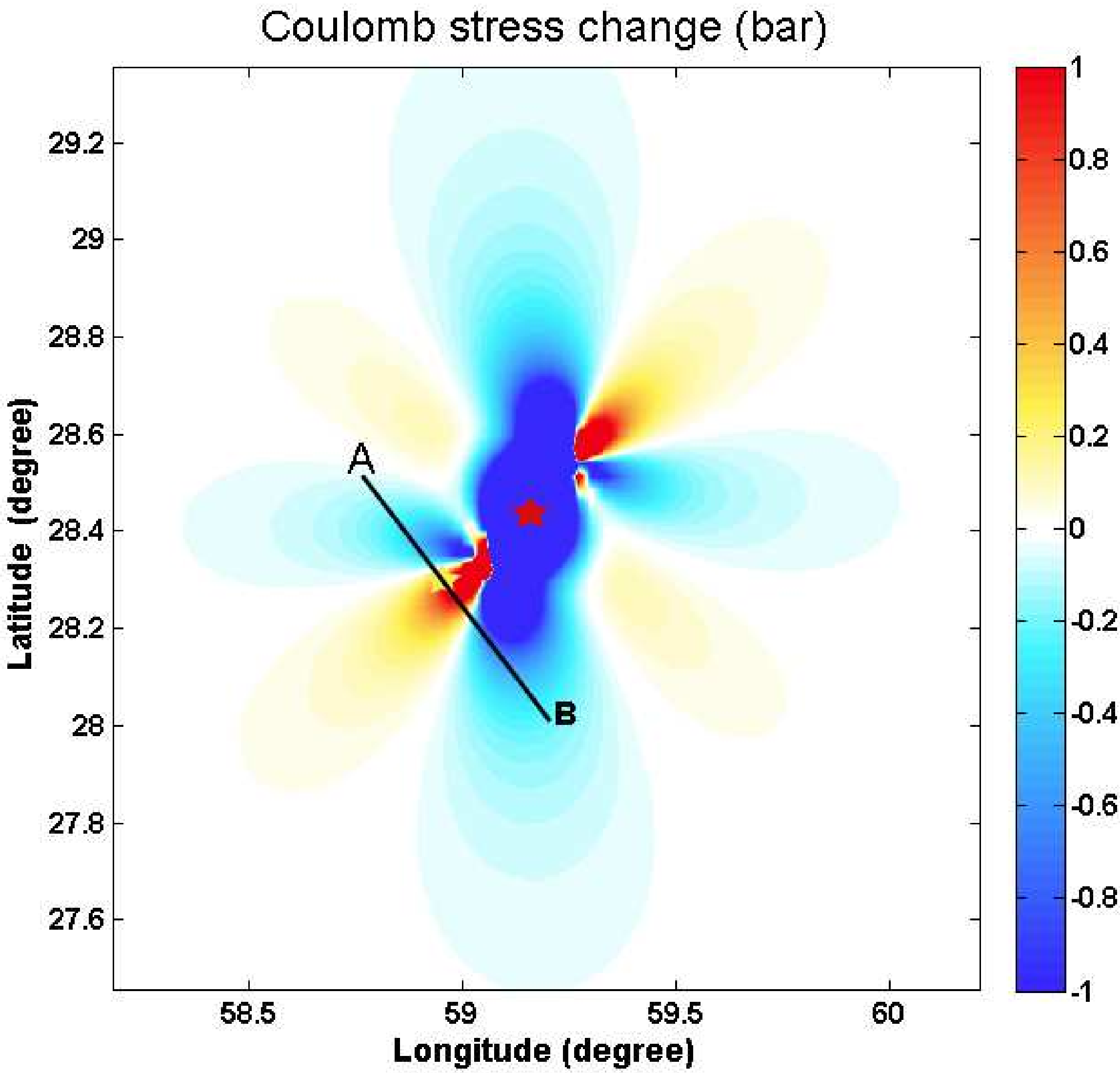
Coulomb stress change (bar)
Latitude (degree)
Longitude (degree)
29.2
29
28.8
28.6
28.4
28.2
28
27.8
27.6
58.5
59
59.5
60
A
B
1
0.8
0.6
0.4
0.2
0
-0.2
-0.4
-0.6
-0.8
-1

Fig.7b

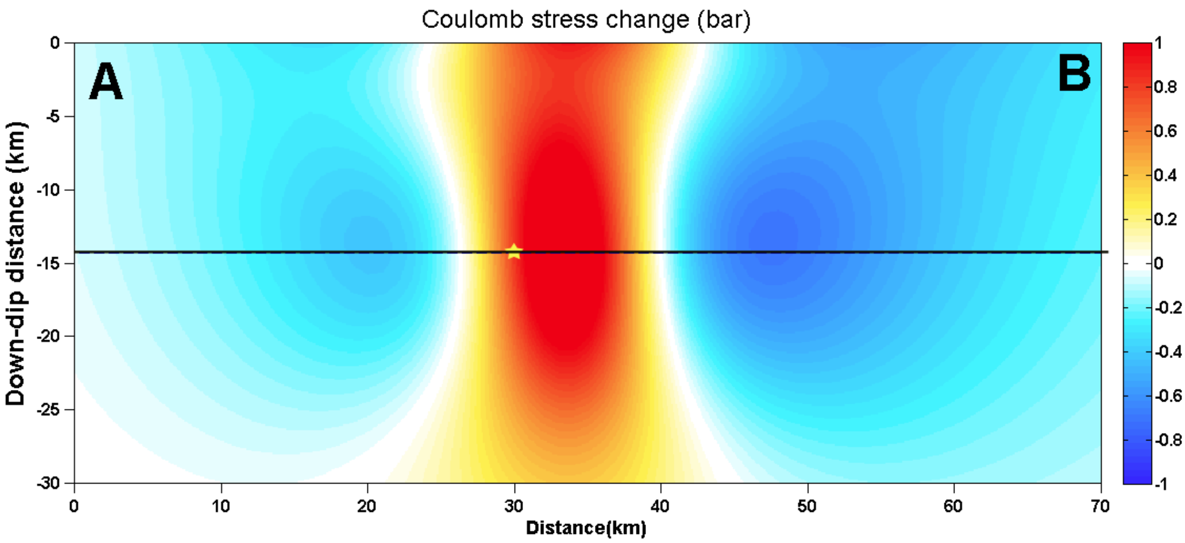
Coulomb stress change (bar)
A
B
Down-dip distance (km)
0
-5
-10
-15
-20
-25
-30
0
10
20
30
40
50
60
70
Distance(km)
1
0.8
0.6
0.4
0.2
0
-0.2
-0.4
-0.6
-0.8
-1

Fig.8

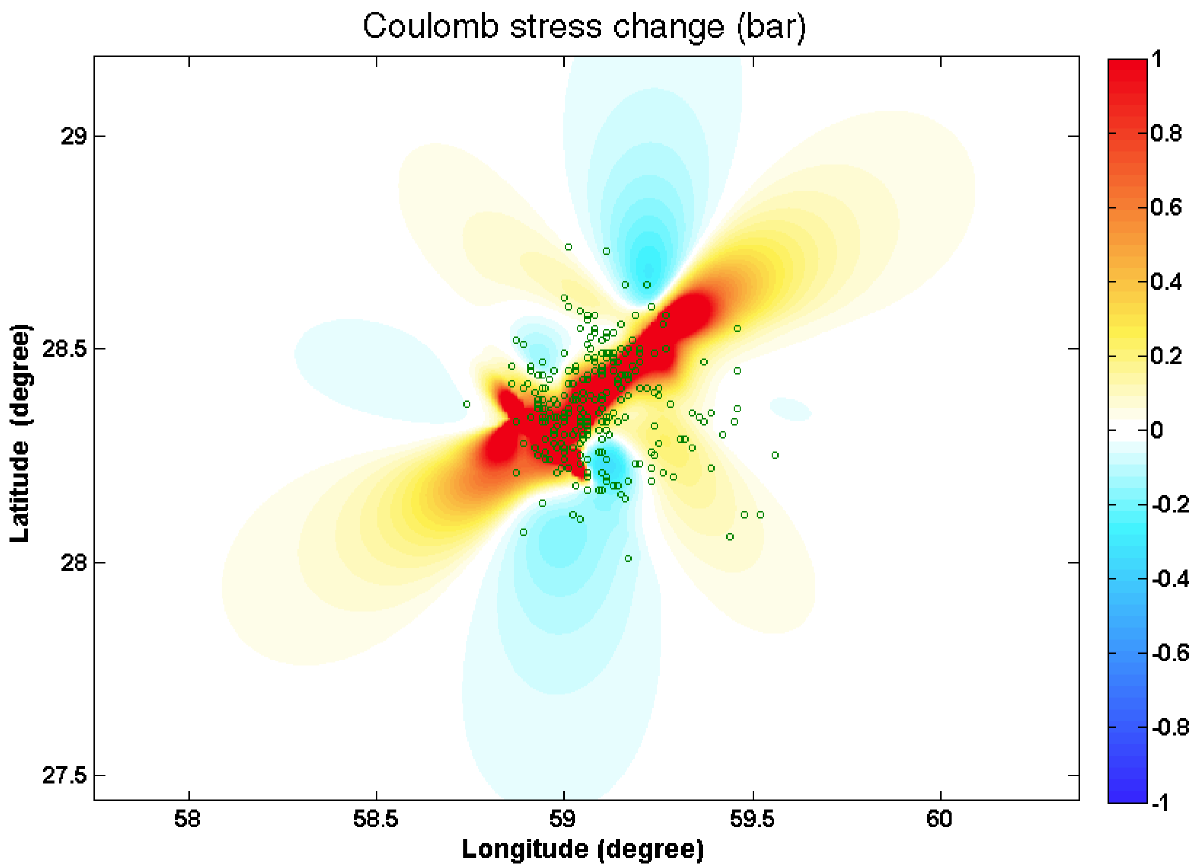
Coulomb stress change (bar)
Latitude (degree)
Longitude (degree)
29
28.5
28
27.5
58
58.5
59
59.5
60
1
0.8
0.6
0.4
0.2
0
-0.2
-0.4
-0.6
-0.8
-1

Highlights

1. This study assesses the aftershock activity of two earthquakes that occurred on December 20, 2010 with magnitude of M_N 6.5 (Global CMT M_w 6.5) and January 27, 2011 with magnitude of M_N 6.0 (Global CMT M_w 6.2) in the Rigan region of southeastern Iran.

2. We concentrated on aftershock activity of this sequence with using Statistical properties of aftershocks (b-value of Gutenberg–Richter relation, partitioning of radiated seismic energy, p-value of modified Omori law, and D_C- value of fractal dimension) and I then use the models to calculate the Coulomb stress change

3. The *b*-values of *b*=0.89±0.08 and *b*=0.88±0.08 were calculated for first main shock and second main shock sequence respectively. This suggests that this region is characterized by large differential stress; the genesis of large aftershock activity in a short time interval gives power this.

4. The *p*-values of 1.1±0.12 and 1.1±0.1 were calculated for the main shocks respectively, which imply fast decay rate of aftershocks and high surface heat flux.

5. A value of the spatial fractal dimension (D_c) equal to 2.34 ± 0.03 and 2.54 ± 0.02 for first and second main shocks sequence respectively, which reveals random spatial distribution and source in a two-dimensional plane that is being filled-up by fractures.